ANL/ET/CP-98089

CRACKING MECHANISM OF TYPE 304L STAINLESS STEEL CORE SHROUD WELDS*

H. M. Chung, J.-H. Park, J. E. Sanecki, and N. J. Zaluzec
Argonne National Laboratory
Argonne, IL 60439, USA

M. S. Yu and T. T. Yang
Institute for Nuclear Energy Research
Lungtan, Taiwan, Republic of China

September 1999

To be published in the Proceedings of 9th International Conference on Environmental Degradation of Materials in Nuclear Power Systems - Water Reactors, August 1-5, 1999, Newport Beach, CA.

---

*Work supported by the U.S. Nuclear Regulatory Commission, Office of Nuclear Regulatory Research.

CRACKING MECHANISM OF TYPE 304L STAINLESS STEEL CORE SHROUD WELDS*

H. M. Chung, J.-H. Park, W. E. Ruther, R. V. Strain, J. E. Sanecki, and N. J. Zaluzec
Argonne National Laboratory
Argonne, IL 60439, USA

M. S. Yu and T. T. Yang
Institute for Nuclear Energy Research
Lungtan, Taiwan, Republic of China

Abstract

Microstructural analyses by advanced metallographic techniques were conducted on mockup welds and a cracked BWR core shroud weld fabricated from Type 304L stainless steel. Heat-affected zones of the shroud weld and mockup shielded-metal-arc welds were free of grain-boundary carbide, martensite, delta ferrite, or Cr depletion near grain boundaries. However, as a result of exposure to welding fumes, the heat-affected zones of the welds were significantly contaminated by fluorine and oxygen which migrate to grain boundaries. Significant oxygen contamination promotes fluorine contamination and suppresses classical thermal sensitization, even in Type 304 steels. Results of slow-strain-rate tensile tests indicate that fluorine exacerbates the susceptibility of irradiated steels to intergranular stress corrosion cracking. These observations, combined with previous reports on the strong influence of weld flux, indicate that oxygen and fluorine contamination and fluorine-catalyzed stress corrosion play a major role in cracking of Type 304L stainless steel core shroud welds.

Key words: stainless steel weld, intergranular stress corrosion cracking, welding contamination, irradiation

Introduction

Failure of welded core internal components such as core shrouds, usually fabricated from Types 304 and 304L austenitic stainless steels (SSs), has increased significantly in boiling water reactors (BWRs). Although BWR core shrouds are subject to relatively low neutron fluence, many vertical and horizontal welds crack by the time they accumulate relatively low fluences of ≈3 x 10^{20} n cm^{-2}. At these low fluences, nonwelded base-metal components would not be considered susceptible to irradiation-assisted stress corrosion cracking (IASCC), which typically occurs after a threshold fluence of ≈5 x 10^{20} n cm^{-2}. Because of this, and in view of the understanding gained from stress corrosion cracking of gas-tungsten-arc-welded (GTA-welded) piping and laboratory-sensitized nonwelded base-metal specimens, most cases of core shroud cracking have been attributed to classical intergranular stress corrosion cracking (IGSCC) of thermally sensitized SS, in which significant grain-boundary carbide precipitation occurs in the heat-affected zone (HAZ) during welding or sensitizing heat treatment. However, the increasing number of cracking incidents in shrouds fabricated from Type 304L SS[1] is difficult to explain on the basis of classical IGSCC, because grain-boundary carbide precipitation would not be expected to occur in low-C SSs. Some investigators hence have suspected that significant grain-boundary Cr depletion could occur in Type 304L SS core shroud welds via a nonequilibrium thermal process or an irradiation-induced process even at very low fluence. The waterside wall of BWR pipings and most small components are welded by the GTA procedure in an inert atmosphere. In contrast, large core internal structures, such as core shrouds, are welded in air by a shielded-metal-arc (SMA) or submerged-arc (SA) procedure, in which weld electrodes coated with F-containing flux are used to produce a plasma shield around the arc-melted plates. In such circumstances, a previous study indicated that the deleterious effects of O and F contamination could play a significant role.[2] Deleterious effects of O on base-metal IASCC have also been reported.[3,4] In this study, to provide a better understanding of the cracking mechanism of Type 304L core shroud welds, microstructural characteristics of unirradiated welds and of a field-cracked Type 304L SS core shroud weld were investigated systematically by chemical analysis, optical microscopy (OM), scanning electron microscopy (SEM), Auger electron spectroscopy (AES), secondary-ion mass spectroscopy (SIMS), and field-emission-gun advanced analytical electron microscopy (FEG AAEM). Results from these studies were then correlated with the SCC behavior of irradiated steels and nonirradiated welds that were contaminated by F or weld fumes.

---

*Work supported by the U.S. Nuclear Regulatory Commission, Office of Nuclear Regulatory Research.

Materials and Experimental Procedures

The composition and types of the stainless steels used to produce mockup welds are given in Table 1. For purpose of systematic comparison, SMA and GTA welds were prepared from Types 304, 304L, and 316 SS. Thicknesses of the solution-annealed base-metal plates of these steels are also given in Table 1. Table 2 describes the neutron fluence and composition of the Type 304L SS BWR-C shroud weld that was investigated in this study. Details of stress corrosion testing and microstructural analysis in a JEOL JAMP-10 automated scanning Auger microscope (SAM) are available elsewhere.[3-5] Microstructural analysis by transmission electron microscopy (TEM) was conducted in either a Vacuum Generator HB-603 FEG AAEM or a JEOL 100CX-II scanning transmission electron microscope (STEM). Ion mapping by Cameca 4F SIMS was conducted with Cs^+ ion as the sputtering and primary beam at 10 kV and 150 nA.

Mockup Core Shroud Welding

To simulate the microstructure of a core shroud weld, mockup SMA welds were prepared from the steel plates described in Table 1. For comparison, GTA welds were also prepared from the same plates. The SMA procedure, which is shown schematically in Fig. 1, uses welding electrodes that are coated with a welding flux. In SA welding, a similar flux is used in powder form to cover the base-metal plate. Consequently, similar impurity contamination occurs in the weld and heat-affected zones (WZs and HAZs) in SMA and SA welds. Vertical welds in a core shroud are usually welded by an SA procedure, whereas horizontal welds are prepared by an SMA procedure. The composition of the SMA welding electrodes, described in ASME Specification Section II SFA 5.4, "Specification for Stainless Steel Electrodes for Shielded Metal Arc Welding," is given in Table 3. The electrode consists of ≈60% coating and ≈40% Type 308 SS. Fluorine was contained in granules of fluorspar dispersed in the silicate binder. Fluorine content in the electrode coating, determined by separate chemical analysis, was ≈2.86 wt.%, and analysis by SEM energy-dispersive spectroscopy (EDS) confirmed the presence of CaF_2. Fluorspar is readily vaporized during welding and produces a plasma shield over the molten steel under the applied high voltage.

The SMA and GTA welds from the 12.7-mm-thick plates were prepared by making 8 and 18 weld passes, respectively. However, SMA welds of the 38-mm-thick plates required as many as 38 weld passes. A schematic diagram of the welding passes and TEM disk locations of the 38-mm-thick plate of Type 304 SS, Heat 19611, is shown in Fig. 2. Weld slag and slag pockets were removed after each welding pass. Weld slags trapped in the weld cusps were removed with a grinding wheel.

Structure and Properties of Mockup Core Shroud Welds

Chemical Analysis Compositions of the SMA and GTA weld HAZs of Type 304 SS Heat C1 were reported elsewhere.[2] While contamination in the GTA weld HAZ was insignificant, the SMA weld HAZ of Types 304 and 304L SS was significantly contaminated by O (up to ≈640 wppm), Mo (up to ≈0.27 wt.%), and F, the elements from the E-308-16 electrode or air. The Type 316 SS SMA weld HAZ lost a significant amount of Mo atoms, most likely through formation of Mo oxides which are volatile at high temperatures.

Analysis by SIMS Distribution of O, F, and other impurities was analyzed by SIMS of the SMA and GTA welds of Type 304 SS, Heat C1 and the SMA weld of the Type 304L SS, Heat C3. Results of mapping, in color, of the secondary ions of O, F, Ca, C, and N from the WZ and HAZ were obtained by using Cs^+ as the primary ion (see Fig. 3). Black, red, orange, and white in the map correspond, respectively, to regions of proportionally higher ion population; black corresponds to no or negligible ions detected, and white corresponds to the highest ion population. For the ion maps given in the figure, the boundaries between the WZ and HAZ are also marked. The results of the SIMS analyses can be summarized as follows:

(a) Oxygen and F contamination was significant in all SMA welds. Oxygen contamination was more pronounced in the WZ than in the HAZ.

(b) GTA welds were not contaminated by F.

(c) Because of repeated exposure to welding fumes, O and F contamination was more pronounced near the surface weld scale than in the midwall of weld HAZ.

Table I. Welding Type, Composition (wt.%), and Thickness of Stainless Steel Plates

ANL Heat ID	Steel Type	Thickness (mm)	Weld Type Investigated	Ni	Si	P	S	Mn	C	N	Cr	Mo
C1	304	12.7	SMA, GTA	8.12	0.50	0.038	0.002	1.00	0.060	0.060	18.11	-
C3	304L	12.7	SMA, GTA	8.91	0.46	0.019	0.004	1.81	0.016	0.083	18.55	-
C21	316	12.7	SMA, GTA	10.24	0.51	0.034	0.001	1.19	0.060	0.020	16.28	2.08
19611	304	38	SMA	8.36	0.48	0.024	0.018	1.69	0.060	0.086	18.35	0.14
M9284	304	38	SMA, GTA	8.12	0.45	0.021	0.011	1.47	0.050	0.055	18.49	0.28

Table II. Composition (wt.%) and Fluence of Cracked BWR Core Shroud Weld

ANL ID of Specimen	Source BWR	Steel Type	Cracked Weld Boat Sample	Composition (wt.%)									Fluence
				Cr	Ni	Mn	C	Nb	Mo	Si	P	S	(10^{19} n·cm^{-2})
507-A and 507-B[a]	BWR-C	304L	H3, ID	18.90	9.36	1.82	0.027	0.064	0.568	0.483	0.024	0.0018	4.6

[a] Composition determined for irradiated sample by electron microprobe analysis, C content from unirradiated plate.

Table III. Composition (in wt.%) of E-308-16 Welding Electrode

Fe	Cr	Ni	Mn	Si	Mo	C	Cu	Nb	V	F	$CaCO_3$	CaF_2	SiO_2	TiO_2	Al_2O_3	Silicate
67.5	20.3	9.7	1.17	0.52	0.39	0.052	0.1	0.02	0.07	2.86	2-8	1-10	1-8	1-12	0-3	<5

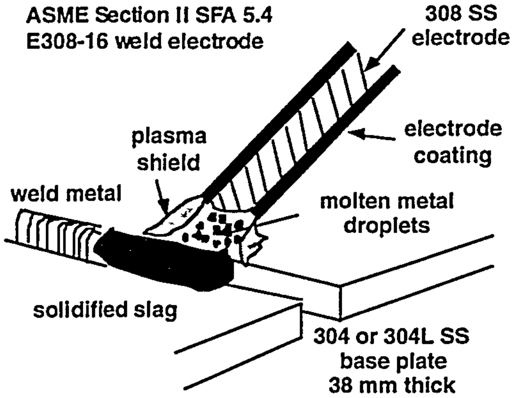

Figure 1: Shielded-metal-arc welding procedure.

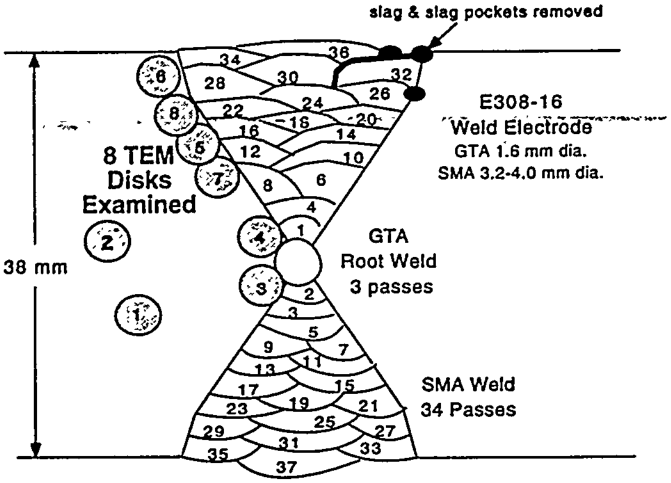

Figure 2: Weld passes and location of TEM disks of Type 304 SS, Heat 19611.

(d) Sparsely populated oxide inclusions were present in the base metal of Type 304 SS, Heat C1. These oxides were rich in F, showing that the base metal contained F in oxides that formed during the ingot-melting process.

(e) Nitrogen and C contamination was insignificant in SMA and GTA welds.

(f) Significant carbide precipitation occurred in the HAZ of the GTA weld. In contrast to oxides, carbides were not enriched by F atoms, a finding that is consistent with the results of previously reported AES analyses of BWR neutron-absorber tubes.[5]

(g) Carbide precipitation was negligible in the HAZ of the SMA weld of Type 304 SS, Heat C1 (≈0.060 wt.% C) and Type 304L SS, Heat C3 (≈0.016 wt.% C). In contrast to GTA welding, thermal sensitization did not occur during SMA welding, even in high-C Heat C1.

(h) Calcium-rich precipitates were present in SMA welds in the WZ and in the HAZ near the fusion line. Most of these precipitates were also rich in O and F. No calcium-rich precipitates were present in GTA welds.

SEM-EDS Because Ca-rich precipitates were absent from GTA welds, it was not likely that we would observe (Ca,Mn)S-type sulfides, which are present in some steels;[5] they are more likely to have been produced in association with the SMA welding procedures. To confirm this, compositions of the Ca-rich precipitates were determined by EDS. The results are shown in Fig. 4. The Ca-rich precipitates were high in O, F, and Si, the same elements that are also high in the flux compound in the weld electrode coating. The composition of the fragile weld scale was similar but contained more Si, K, O, and Ti. Therefore, it is obvious that Ca-oxyfluoride-type precipitates form in association with SMA welding. After each welding pass, the weld slag pockets were removed from weld cusps with a grinding wheel, and this process may have assisted the formation of the Ca-rich precipitates by impregnating particles of broken weld scale. The Ca-rich inclusions dissolved readily when in contact with water during either SSRT testing at 288°C or polishing at room temperature. When the specimen surface was polished in an oxalic acid solution, however, the inclusions did not dissolve. These observations indicate that the Ca-oxyfluoride-type inclusions are soluble in reactor coolants and hence could accelerate the release of F ions into the crack tip.

Analysis by TEM The absence of carbide precipitates in the SIMS maps of the HAZ of the SMA weld of the L-grade Heat C3 (≈0.016 wt.% C) was expected (see Fig. 3). However, a similar observation for the high-C Heat C1 (≈0.060 wt.% C) was a major surprise, because, in contrast to a GTA weld, this observation means that an SMA weld of Type 304 SS would not exhibit thermal sensitization via grain-boundary carbide precipitation. Therefore, grain-boundary carbides were characterized extensively by TEM to investigate more directly the behavior of thermal sensitization in the GTA vs. SMA welds. Disks for TEM analysis were punched from the HAZ and base metal, as illustrated in Fig. 2. Grain-boundary carbides were characterized by the combination of bright-field imaging, tilting, selected-area-diffraction (SAD) analysis, and dark-field imaging. Results of the analyses are summarized in Table IV and Fig. 5. For Type 304 SS, many $M_{23}C_6$ carbides were observed on the grain boundaries of the HAZ of the GTA welds. In contrast, carbides were not present on or near grain boundaries of the HAZ of all SMA welds, regardless of steel type, C content, and location of the TEM disks relative to the free surface or fusion line.

Table IV: Summary of TEM Characterization of Grain-Boundary Carbide Precipitation in HAZs of SMA and GTA Mockup Welds and BWR-C Core Shroud H3 Weld.

Steel Type	Heat or Specimen ID	Bulk Carbon (wt.%)	Plate Wall (mm)	Weld Type	Carbides Detected by TEM	Carbides Detected by SIMS
304	C1	0.060	12.7	SMA	**none**	**none**
304	C1	0.060	12.7	GTA	many	many
304L	C3	0.016	12.7	SMA	**none**	**none**
304L	C3	0.016	12.7	GTA	none	–
316	C21	0.060	12.7	SMA	**none**	–
316	C21	0.060	12.7	GTA	some	–
304	19611	0.060	38	SMA	**none**	–
304	19611 SMA weld annealed	0.060	38	SMA, 620°C 24 h	**none**	–
304	M9284	0.050	38	SMA	**none**	–
304	M9284	0.050	38	GTA	many	–
304L shroud	507-A	0.027	38	H3 weld SMA	–	–
304L shroud	507-B	0.027	38	H3 weld SMA	none	–

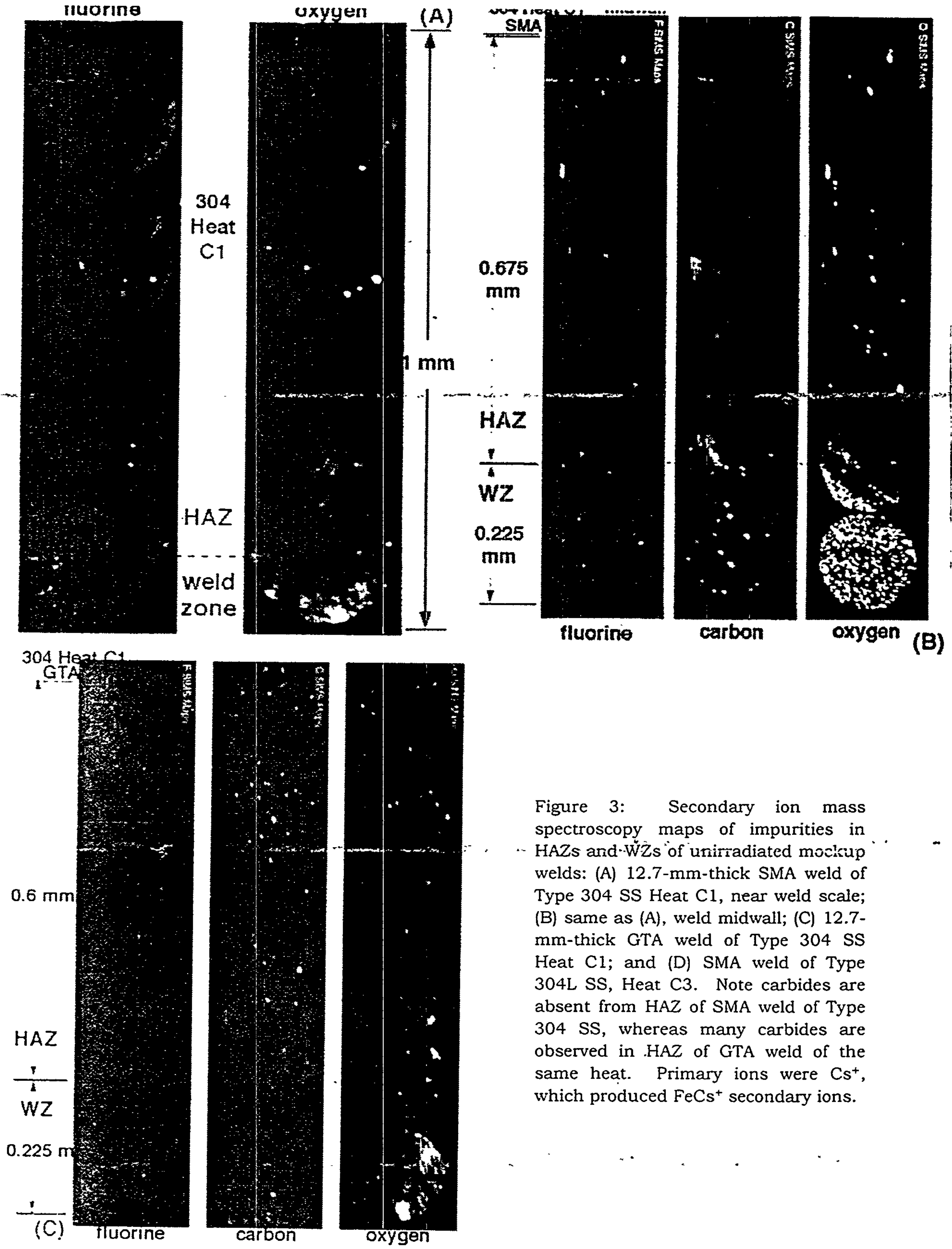

Figure 3: Secondary ion mass spectroscopy maps of impurities in HAZs and WZs of unirradiated mockup welds: (A) 12.7-mm-thick SMA weld of Type 304 SS Heat C1, near weld scale; (B) same as (A), weld midwall; (C) 12.7-mm-thick GTA weld of Type 304 SS Heat C1; and (D) SMA weld of Type 304L SS, Heat C3. Note carbides are absent from HAZ of SMA weld of Type 304 SS, whereas many carbides are observed in HAZ of GTA weld of the same heat. Primary ions were Cs^+, which produced $FeCs^+$ secondary ions.

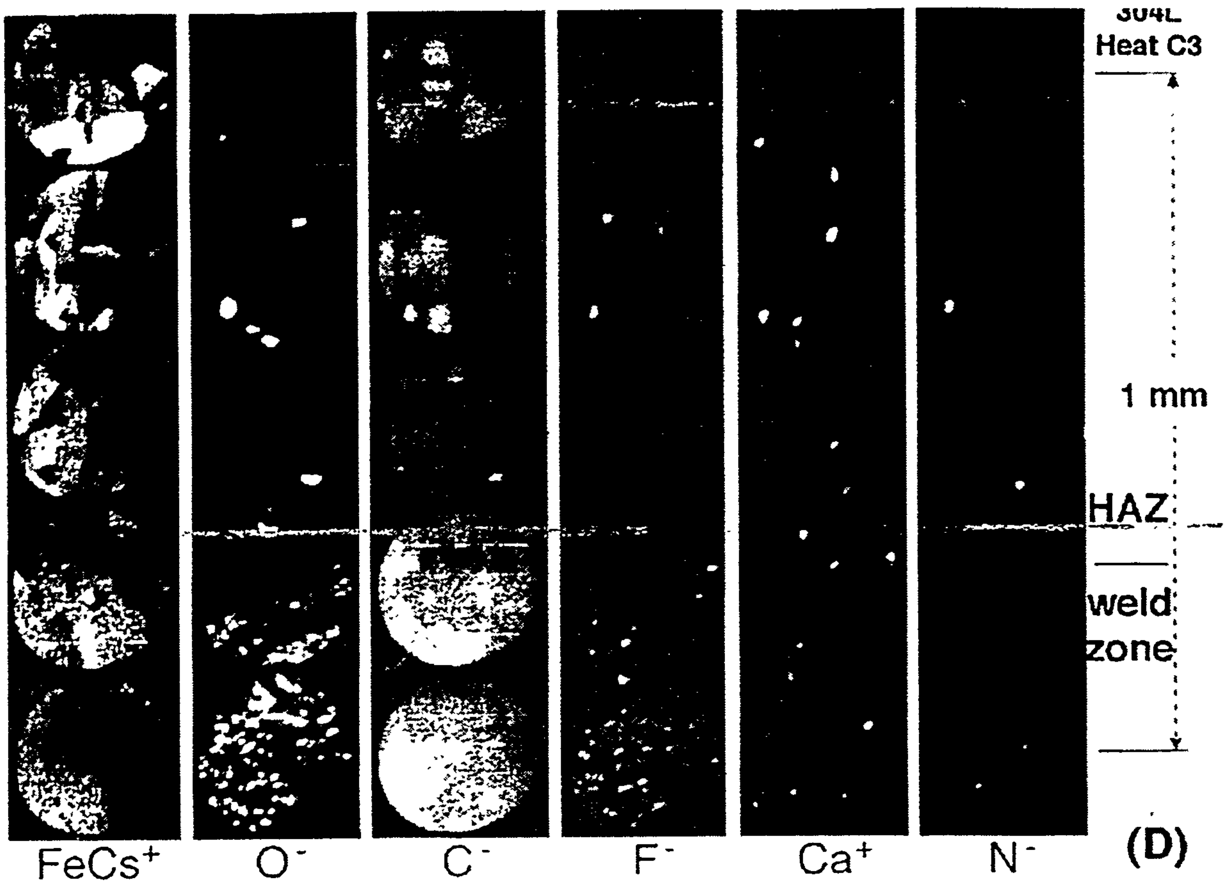

Figure 3 Continued.

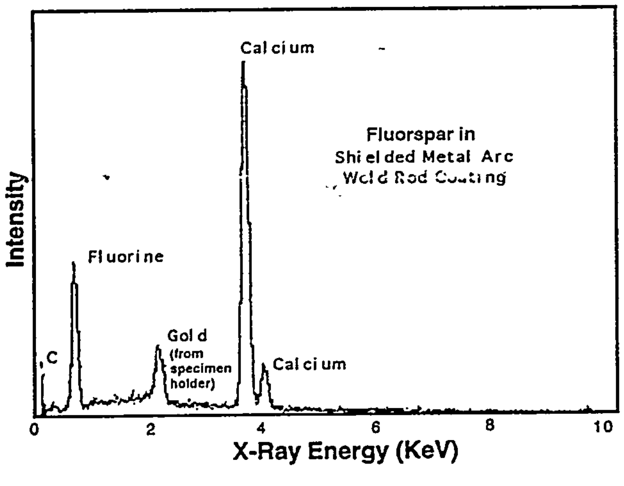

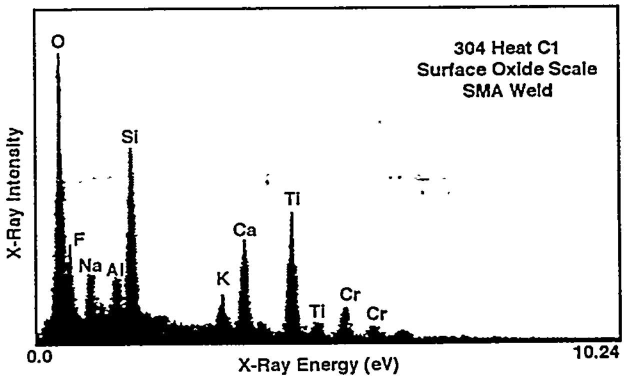

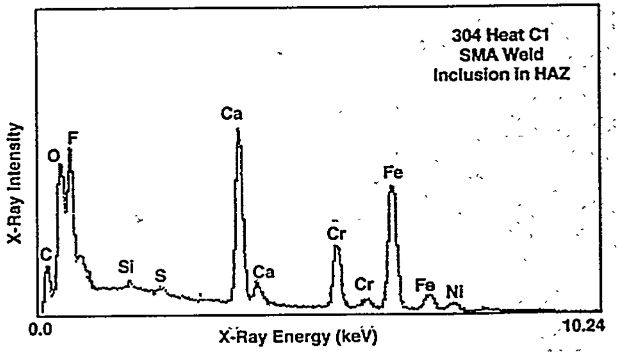

Figure 4: Compositions determined by EDS: (top left) granule of CaF_2 fluorspar in welding electrode coating, (top right) surface weld scale, and (bottom right) Ca-rich precipitate in HAZ in mockup SMA weld of Heat C1.

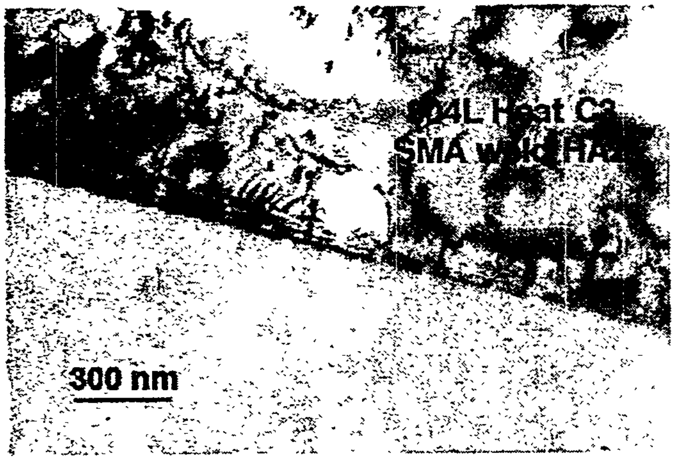

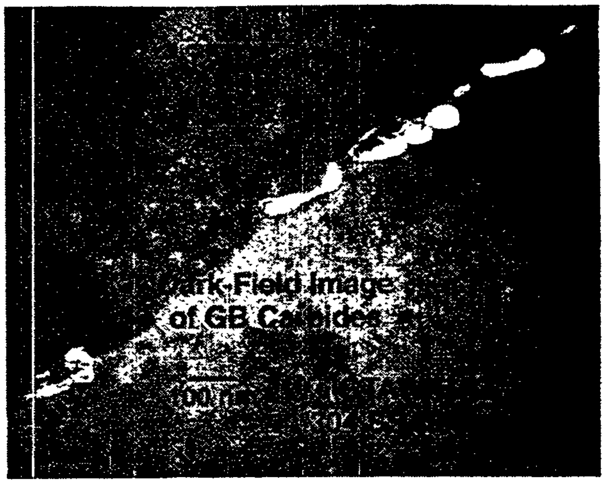

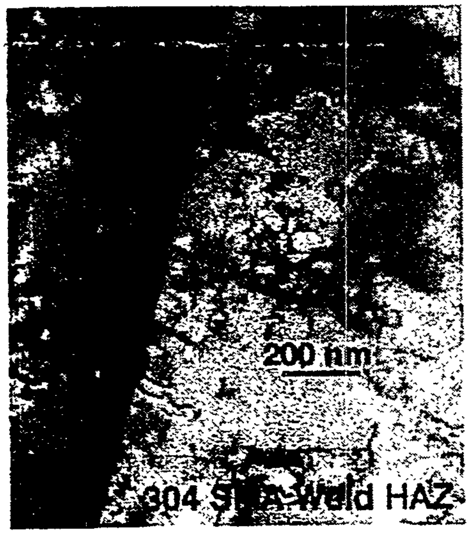

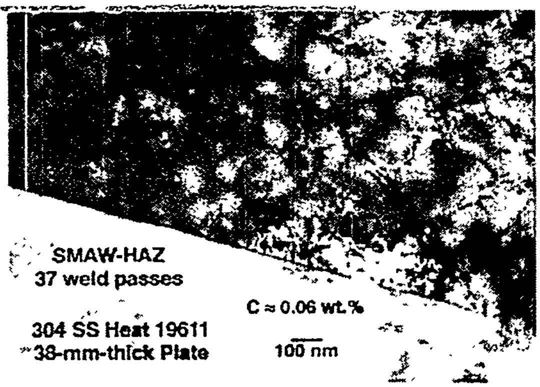

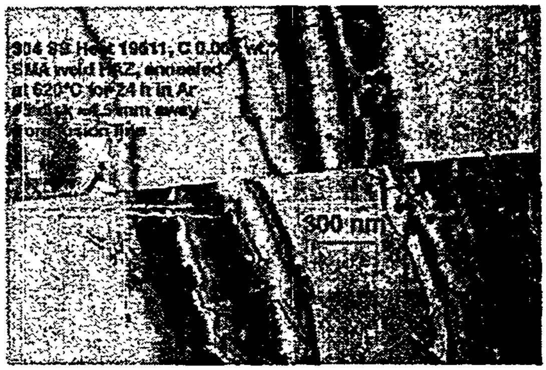

Figure 5: Microstructure of grain boundaries of HAZs of nonirradiated mockup welds: (top left) SMA weld, Type 304L SS Heat C3, (top right) dark-field image of carbides in GTA weld, Type 304 SS Heat C1, (middle left) SMA weld, Type 304 SS Heat C1, (middle right) SMA weld, Type 304 SS Heat 19611; (bottom right) SMA weld, Heat 19611, annealed at 620°C for 24 h in Ar.

As a further experiment, the SMA weld of high-C Heat #19611 (C content ≈0.060 wt.%) was annealed at 620°C for 24 h in Ar. The surface weld scale was removed before the annealing treatment. After the postwelding annealing, five TEM disks were prepared from the 1-mm-thick strip beneath the free surface for characterization of grain-boundary carbides, four from the HAZ (disk center 1.5-4.5 mm from the fusion line) and one from the base metal (disk center 7.5 mm from the fusion line). A very limited amount of grain-boundary carbides was observed in only the last disk. In that disk, only ≈8% of the total length of seven grain boundaries in the specimen was covered with carbides. However, carbides were not present on or near grain boundaries in any of the four disks that were excised from the HAZ (Fig. 5). Results of this experiment show that classical thermal sensitization in SMA welds does not occur, even after postwelding "sensitization treatment".

In summary, for heats of Types 304 and 316 SS, grain-boundary carbides were observed in the HAZs of all GTA welds, whereas grain-boundary carbides were absent from the HAZ of the SMA welds. These observations show that susceptibility to thermal sensitization is negligible in SMA welds, a major contrast to the behavior of GTA welds. It is most likely that high O or OF contamination associated with SMA welding suppresses grain-boundary carbide precipitation because the affinity of Cr for O or OF is stronger than the affinity of Cr for C atoms.

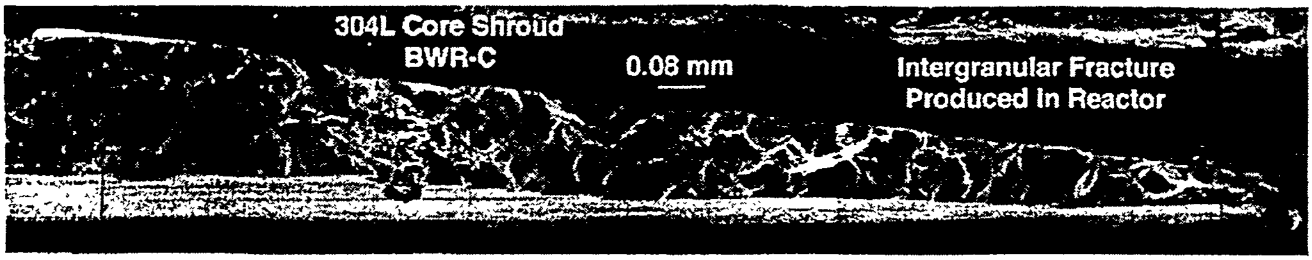

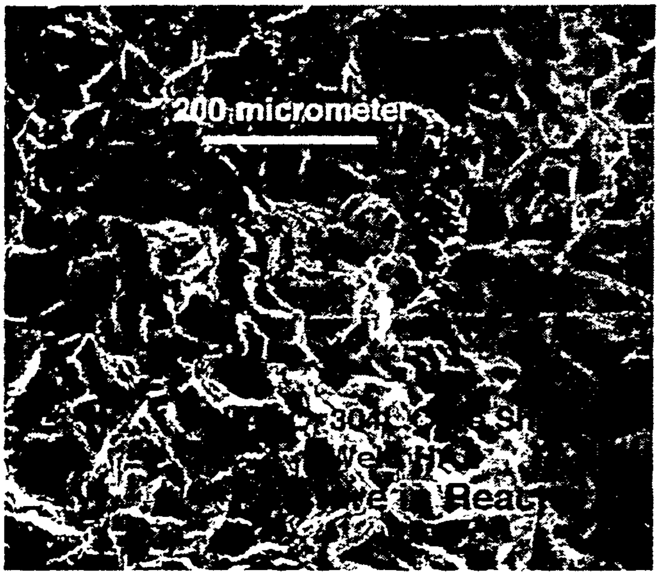

Figure 6. SEM fracture surface morphology of Type 304L BWR-C core shroud weld, in-reactor fracture in (top) 507-B and (bottom) 507-A specimens.

Fracture Behavior and Microstructure of Type 304L SS BWR-C Core Shroud Weld

SEM Fractography Microstructures of two boat samples from the field-cracked BWR-C core shroud weld, irradiated to a fluence of 4.6 x 10^{19} n·cm^{-2} (E >1 MeV), were characterized by SEM, FEG-AAEM, and AES. Regions of clean fracture surface morphology could be found near the tight crack tip. The fracture surface (Fig. 6) does not show typical intergranular fracture morphology; it appears to contain a significant fraction of ductile tearing in addition to intergranular separation.

FEG-STEM Analysis Neither carbide nor martensite or delta-ferrite thin film was detected on grain boundaries of HAZ specimens that were characterized by an HB603 FEG-AAEM. As expected, the Type 304L SS weld HAZ was not thermally sensitized. However, globular internal oxides, ≈200-500 nm in diameter, were often observed near grain boundaries (Fig. 7). Furthermore, EDS spectra obtained away from such oxides showed that grain-boundary Cr depletion by a thermal or irradiation-induced process was negligible (Fig. 7). Therefore, cracking of this core shroud weld cannot be explained on the basis of either classical IGSCC or IASCC.

AES Analysis of Internal Oxides and Oxygen. Internal oxidation behavior of the core shroud weld HAZ was analyzed by AES and OM (Figs. 8-10). Clean, in-situ fracture surfaces were produced at ≈23°C in the ultrahigh vacuum of the scanning Auger microscope. A typical example of the clean in-situ fracture surface is shown in Fig. 8. The figure shows intergranular fracture surfaces and many fine particles (≈100-1500 nm in diameter) on the grain boundaries. These particles were either Cr oxides or Fe-Ni spinel oxides (Fig. 8), indicating that O concentration near grain boundaries of the HAZ was very high. Overall distribution of these grain-boundary oxides, usually ≈3,000-15,000 nm apart, could be estimated better by SAM (Fig. 8) than by TEM (Fig. 7).

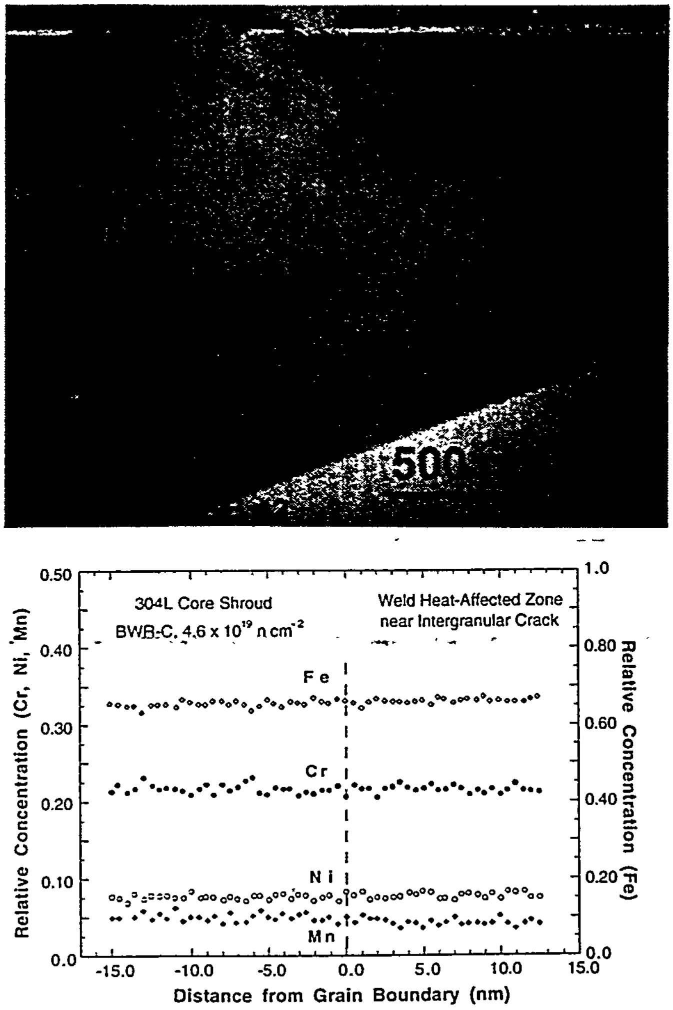

Figure 7. (Top) bright-filed TEM image, showing internal oxide near grain boundary of BWR-C core shroud weld HAZ of Specimen 507-B and (bottom) Fe, Cr, Ni, and Mn distributions near grain boundary that were measured in region away from an internal oxide.

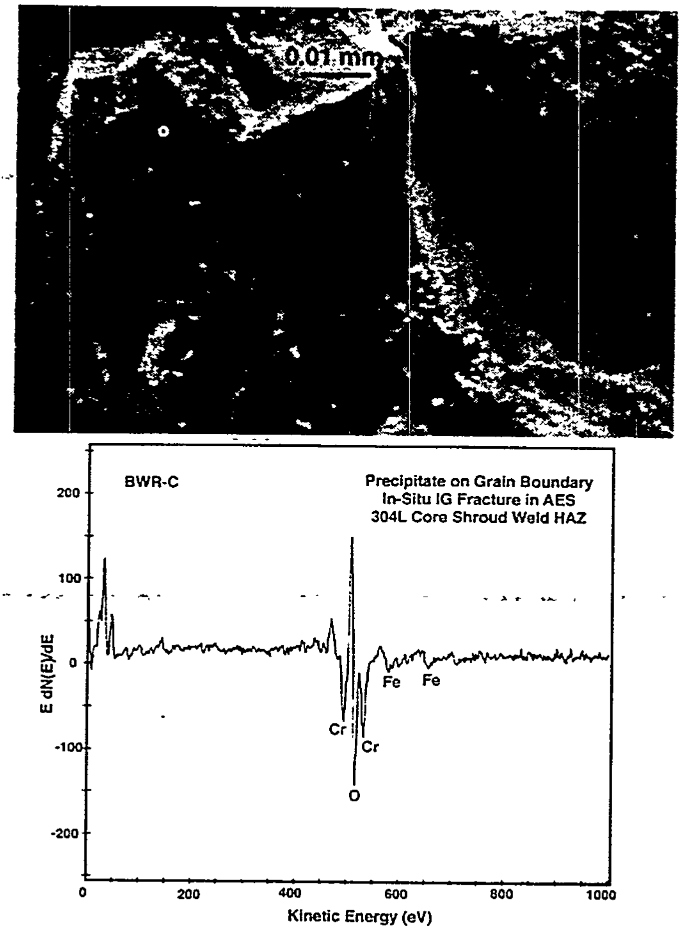

Figure 8. AES in-situ fracture surface morphology in HAZ of Type 304L BWR-C core shroud weld, (fracture produced at ≈23°C in ultrahigh vacuum, top) and signal from particle denoted "ppt," showing a Cr oxide (bottom).

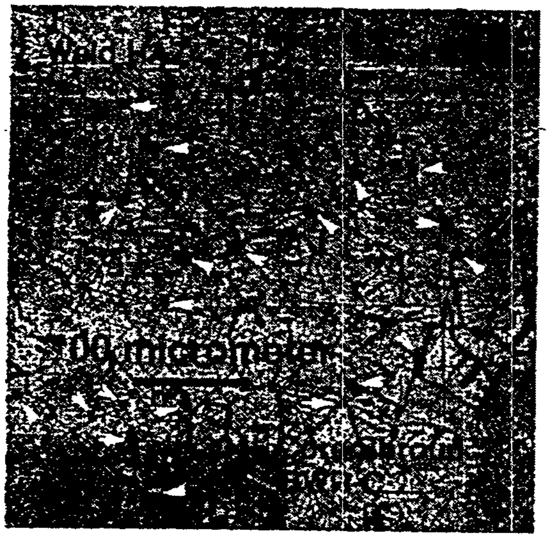

Figure 9. Optical photomicrograph of HAZ near fracture surface of cracked H3 weld in BWR-C core shroud, Type 304L SS. White arrows denote oxide inclusions located near or on grain boundaries.

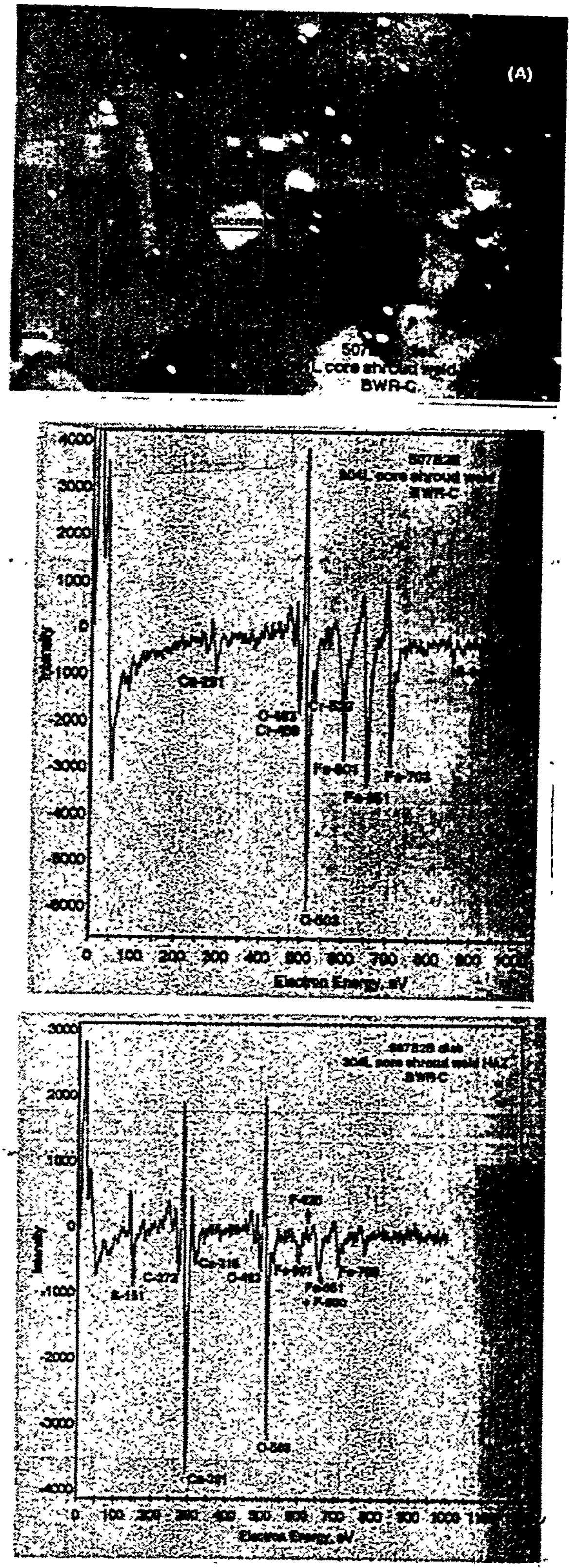

Figure 10. AES image of polished and Ar-ion-sputtered HAZ near fracture surface of BWR-C core shroud weld (top). Spectra from Fe-Cr oxide and CaO, denoted as "oxide" or "CaO," are shown in the middle and bottom inset, respectively.

Evidence for the presence of numerous grain-boundary oxide particles could also be obtained from AES analysis of polished specimens. An optical photomicrograph of a polished surface, obtained from the H3 weld HAZ of Type 304L SS BWR-C core shroud, is shown in Fig. 9. Besides grains and annealing twins, numerous inclusions are visible; many are on or near grain boundaries. The inclusions on or near grain boundaries are denoted with white arrows in the figure. To identify the inclusions, the polished specimen was analyzed by AES after sputtering a selected area with Ar ions for ≈300 s. On the surface of the sputtered specimen, many light-contrasted inclusions were visible in a secondary-electron image (Fig. 10). The light contrast indicates that the inclusions are insulators and are charged electrically. Most of the inclusions were Fe-, Cr-, or spinel-type oxides. Some of the inclusions were identified as CaO, a finding that is consistent with the observation of Ca oxyfluorides in the mockup core shroud weld by SIMS mapping (Fig. 3D). No carbides were observed. The presence of metal oxides and CaO inclusions in both BWR-C core shroud and the mockup SMA weld HAZ is consistent with the premise that significant contamination by O and Ca occurred during welding.

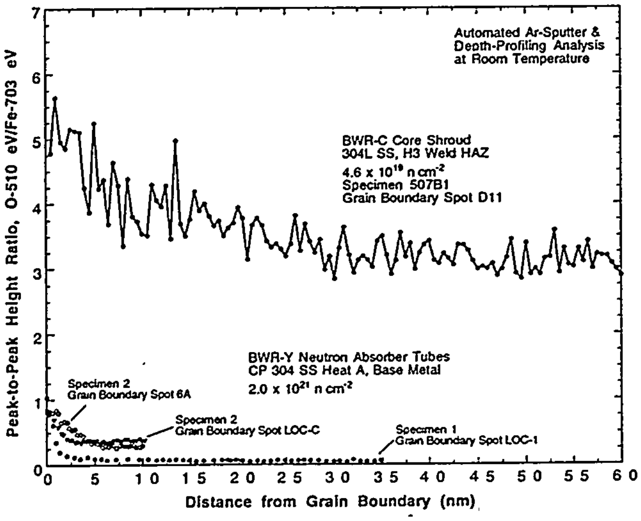

Figure 11. Peak-to-peak height ratio of O at ≈510 eV to Fe at ≈703 eV as function of distance from grain boundary, BWR-C core shroud weld HAZ, Specimen 507-B. Similar data for BWR neutron absorber tubes are shown for comparison.

The dense oxides that were observed on the grain boundaries (Figs. 8 and 9) and grain-boundary triple points (Fig. 9) indicate that O atoms are concentrated on grain boundaries of the weld HAZ of the BWR-C core shroud. To obtain more direct evidence for O distribution near grain boundaries, automated depth-profiling analysis was conducted on a grain-boundary spot at least ≈5,000 nm (≈10 times greater than the radius of the beam[5]) away from oxides. The selected spot is denoted with a white circle in the fracture surface in Fig. 8. The result is shown in Fig. 11. For intergranular or ductile fracture surfaces produced in-situ in neutron-irradiated base-metal components (such as BWR neutron absorber tubes[4]), O distribution near a grain boundary was difficult to determine because significant chemisorption of O occurred (at ≈23°C) as a result of exposure to the ultrahigh-vacuum environment of SAM. This artifact O-rich layer, ≈2-3 nm thick, is readily removed after only several seconds of Ar ion sputtering. Subsequently, the O signal reaches an asymptotic level that corresponds to the O concentration of the bulk material[4] (Fig. 11). For such situations, the degree of grain-boundary O segregation could not be determined by AES. It was also difficult to determine O distribution by FEG-STEM EDS because the K line of O and the L lines of Cr and Fe virtually overlap. In contrast to base-metal components, O chemisorption on in-situ-fractured grain-boundary surfaces of the core shroud weld HAZ was negligible, and no sudden decrease of O signal was observed during the initial seconds of sputtering. We believe this is because the core shroud weld HAZ contains an unusually high concentration of O (Fig. 11). The profile of the 510-eV peak of O, normalized with respect to the primary peak of Fe at 703 eV, shows that O concentration is significantly higher on or near the grain boundary than in the grain matrix.

AES Analysis of Fluorine. The AES signals of F in steels can be easily overlooked because the primary dN(E)/dE peak is hidden behind the strong Fe peak, even though F gives rise to a very weak secondary peak at ≈625 eV.[4] Because of this inherent difficulty, AES is not a sensitive technique for analysis of F in Fe-base alloys. Nevertheless, F signal intensities at ≈625 eV were determined for a core shroud weld HAZ, as well as ductile and intergranular fracture surfaces and precipitates in several irradiated BWR tube and sheath components that were fabricated from solution-annealed Types 304 and 348 SS (Fig. 12). The results were compared with those obtained by SIMS of mockup SMA welds.

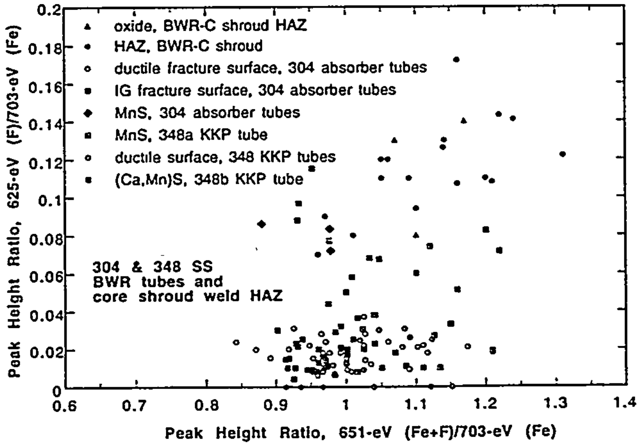

Figure 12. Intensities of Auger electrons of F at ≈625 eV and F plus Fe at ≈651 eV from BWR-C core shroud weld HAZ, Specimen 507-B, and ductile and intergranular fracture surfaces and precipitates contained in base-metal BWR components.

For most spots on the fracture surfaces of the base-metal components, the F signal at ≈625 eV was negligible; therefore, only those spots that give rise to a signal distinctively higher than the noise level were included in Fig. 12, which shows that the F content of oxides and sulfides is relatively higher than that in the grain matrices of the base metals. No evidence for F enrichment of carbides was observed. These observations are consistent with the results of the SIMS ion mapping shown in Fig. 3. The greater concentrations of F in oxides also appear to be consistent with the results of Shimizu et al.,[6] who showed by SIMS that F is readily incorporated into Ta oxides at ambient temperature and that a large number of OF complexes are formed.

The results in Fig. 12 also show that the F level is relatively higher in the grain matrices of the shroud weld HAZ than in the grain matrices of other nonwelded irradiated components that were fabricated from a solution-annealed base metal. This finding is also consistent with the results of SIMS analyses of SMA welds (Fig. 3). However, F distribution on or near grain boundaries could not be determined by AES because of the problem associated with the overlap of Fe and F primary signals.

Microhardness Measurement To determine the thickness of the cold-worked layer of the BWR-C shroud weld specimens, microhardness was measured as a function of depth from the finished free surface in the HAZs. The results are shown in Fig. 13. Hardness profiles measured at ≈0.13, ≈3.0, and ≈3.2 mm away from the fracture surface were similar. Also shown in the figure are similar profiles of specimens from Type 304 SS BWR-D and -Q core shroud weld HAZs. Hardness profiles of BWR-C and BWR-Q shroud welds were very similar, decreasing from ≈380 VHN at the surface to ≈180 VHN at a depth >0.6 mm. This result shows that the thickness of the cold-worked layers in the two specimens is no more than ≈0.6 mm. However, even though the shroud support rings in the BWR-D and -Q had been fabricated from the same heat of Type 304 SS, the cold-worked layer in the former was significantly thicker (≈1.5 mm) and microhardness was significantly higher (500-220 HVN) than in the latter. This finding indicates that the weld surfaces were finished by different methods.

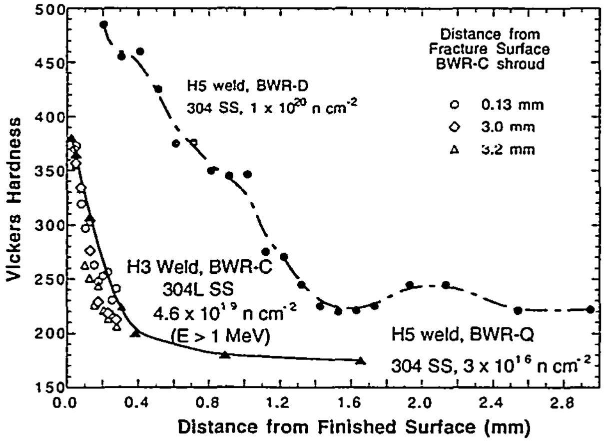

Figure 13. Microhardness profiles of cracked weld HAZs in three BWR core shrouds.

Discussion

Microstructural characteristics of the cracked Type 304L core shrouds weld HAZ can be summarized by: (a) absence of carbides on or near grain boundaries, (b) absence of martensite or delta-ferrite thin film on grain boundaries, (c) presence of dense dislocations, (d) significant O contamination and dense precipitation of fine oxides on grain boundaries and grain-boundary triple points, (e) no or negligible Cr depletion in grain-boundary regions away from oxides, (f) higher concentration of O on grain boundaries, (g) significant F contamination, and (h) an ≈0.5-mm-thick cold-worked surface layer.

Results obtained from the microstructural and microchemical analyses of the mockup nonirradiated SMA welds and field-cracked core shrouds were essentially the same. Considering these observations, it is difficult to explain the core shroud weld cracking on the basis of either classical IGSCC, in which thermal sensitization by grain-boundary carbide precipitation plays the key role, or the grain-boundary Cr-depletion model of IASCC.

In the meantime, fluorine-assisted intergranular SCC has been reported for unirradiated austenitic stainless steels[7-12] and brass.[13] In most of the reported experiments, higher susceptibility to intergranular SCC was caused by fluoride ions that were added intentionally to the water. However, in other experiments, the only source of F that produced higher susceptibility to intergranular SCC was the weld-fume contamination in flux-welded steels.[7,10,11] In the latter investigations, however, microstructural or microchemical characterization that may have provided a better understanding of the mechanism of fluorine-assisted intergranular SCC was not conducted. Although no direct evidence of grain-boundary carbide precipitation was observed, it was assumed implicitly in these investigations that F contamination in flux-welded steels exacerbates the susceptibility of HAZs to classical IGSCC.[7,10] Results of the direct microstructural characterization in the present investigation do not support this assumption. That is, the mechanism of intergranular SCC of weld-fume-contaminated HAZs of flux-welded steels, such as core shroud welds, appears to differ fundamentally from the mechanism of F-assisted IGSCC of sensitized nonwelded (i.e., base metal) steels.

The present investigation shows that significant F contamination of core shroud welds occurs in association with O contamination. The O and F contamination characteristics that were observed in the mockup SMA weld and the Type 304L SS BWR core shroud weld were similar. The tandem contamination of O and F explains well the previous reports by several investigators that welding fume contamination or a surface oxide layer or weld slag strongly exacerbates the susceptibility of flux-welded steels to IGSCC.[7,10,11] Results from previous SSRT tests on neutron absorber tubes[4] also appear to be also consistent with the results of the bend-beam experiments reported in Ref. 7 and 10, that is, F contamination in oxide-covered or O-contaminated steel exacerbates susceptibility to IG stress corrosion cracking.

Evidence of higher O content in the HAZ was higher on grain boundaries than in the base metal of core shroud welds was observed. Conclusive evidence for significant F contamination in the mockup and core shroud weld HAZs was also observed. If we consider the direct association of O and F contamination and segregation of O to grain boundaries in the core shroud weld HAZ, this type of intergranular SCC that is caused by material contamination by O and F (in the absence of grain-boundary carbide precipitation or Cr depletion) would be appropriately termed "oxyfluorine-assisted" SCC. In this type of SCC, a synergism among O, Cr, and F appears to play a primary role, and susceptibility to intergranular SCC is strongly influenced by the degree of O segregation to grain boundaries and by the degree of F contamination in the HAZ. This is because higher O on grain boundaries is conducive to more Cr bound to O, and possibly more F segregated to grain boundaries. This condition, which is conducive to higher F ion and lower Cr ion concentrations in the crack tip water, allows F to play a strong catalytic role in metal dissolution at the crack tip.

The presence of Ca oxyfluoride precipitates appears to accelerate this process because the precipitates dissolve readily in water, thereby releasing F more rapidly in the crack tip water. This effect will promote cracking very close to the fusion line in core shroud welds.

The following model is proposed to explain the mechanism of oxyfluorine-assisted SCC; it is based on a synergism among O, Cr, and F. The catalytic roles of halide ions, in particular Cl and F, in accelerating aqueous corrosion of Fe and steels are well known. This role has been known to be strongly influenced by the concentration of Cr ions in water.[14] The acceleration of corrosion has been attributed to the orders-of-magnitude faster rate of formation of a ligand complex between the Fe-halide and water than the rate of formation of a similar complex between halide-free Fe and water.[14] A similar effect can be postulated for the reaction rates of the formation of F-containing (fast) and F-free (slow) ligand complexes of $[FeF(H_2O)_5]^+$ and $[Fe(H_2O)_6]^{2+}$, respectively. A free F ion is then released from the labile complex $[FeF(H_2O)_5]^+$ in water when H_2O replaces the F atom in the complex. This cycle can be expressed by:

Fe (lattice) + $6H_2O = [Fe(H_2O)_6]^{2+} + 2e^-$
reaction rate slow (1)

Fe–F (F chemisorbed) + $5H_2O = [FeF(H_2O)_5]^+ + e^-$
rate fast (fast dissolution of Fe) (2)

$[FeF(H_2O)_5]^+$
labile in water, because

$[FeF(H_2O)_5]^+ + H_2O = [Fe(H_2O)_6]^{2+} + F^-$
reaction fast, F ion released (3)

Then, the released F^- ion again drives the fast reaction (Eq. 2) to form another $[FeF(H_2O)_5]^+$ complex. This cycle repeats itself, leading to a classical catalytic role for F.

However, the reaction chain is broken when the concentration of Cr ions in crack tip water is high, because nonlabile $[CrF(H_2O)_5]^+$ is formed rapidly but remains inert in water. Therefore, F remains trapped in $[CrF(H_2O)_5]^+$ in the water, preventing the catalytic role of F. This process is expressed:

Cr (lattice) + $6H_2O = [Cr(H_2O)_6]^{2+} + 2e^-$
reaction slow (4)

Cr–F (F chemisorbed) + $5H_2O = [CrF(H_2O)_5]^+ + e^-$
rate fast, fast dissolution of Cr (5)

$[CrF(H_2O)_5]^+$
nonlabile, because

$[CrF(H_2O)_5]^+ + H_2O = [Cr(H_2O)_6]^{2+} + F^-$
reaction slow (6)

Therefore, F atoms are trapped in $[CrF(H_2O)_5]^+$, and hence are prevented from participating in the fast reaction (Eq. 2), because formation of Fe-F (i.e., F chemisorbed on Fe) is minimized.

When the concentration of O on grain boundaries is high (as in the Type 304L core shroud weld HAZ), Cr and O are bound chemically on the crack tip surfaces. Thus, Cr dissolution is suppressed, and the concentration of Cr ions in the crack tip water will be low. Then, the F ion concentration in the crack tip water will be higher and, as depicted in Fig. 14, the catalytic role of F will be in full force. Thus, susceptibility to oxyfluorine-assisted SCC will be strongly influenced by O on grain boundaries, because higher O on grain boundaries is conducive to higher F and more Cr bound to O on the grain boundaries, and hence higher F ion and lower Cr ion concentrations in the crack tip water. Higher concentration of F on grain boundaries is, however, not necessarily a prerequisite condition for oxyfluorine intergranular SCC. The two essential and necessary conditions for the process to occur are material contamination by F and a higher concentration of O on grain boundaries. Depending on the degree of these three processes, the degree of susceptibility to IG stress corrosion cracking will be strongly influenced from one region to another. This seems to be the case for the fracture surface morphologies shown in Fig. 6. In the worst case, cracking can occur significantly farther from the fusion line in a core shroud weld than in a GTA weld.

The model depicted in Fig. 14 also provides a good explanantion for F-assisted IGSCC of sensitized nonwelded material, i.e., cracking of a base metal in presence of fluoride ions in water in which grain-boundary carbide precipitation occurs significantly.[7-12] When F contamination is present and grain boundaries are significantly depleted of Cr by an irradiation-induced process, as in the case of the neutron absorber tubes reported in Ref. 4, the model also predicts susceptibility to IG stress corrosion cracking.

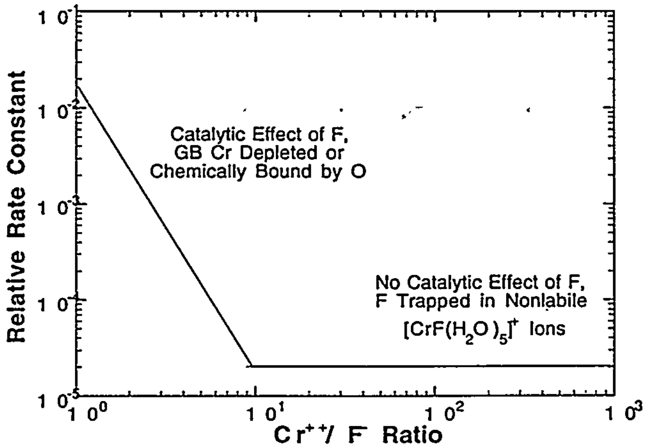

Figure 14. Schematic illustration of effects of O and F on grain boundaries and Cr ion in crack-tip water on oxyfluorine-assisted SCC

From the findings in this study, it is difficult to support a mechanism in which the presence of a cold-worked layer alone (in absence of O and F contamination) is sufficient to produce IG cracking in either Type 304L or Type 304 SS core shroud welds. In fact, the IG stress corrosion cracking in the bend-beam specimens of the flux-welded steels, reported in Refs. 7, 10, and 11, occurred in the absence of any cold-worked layer. Therefore, it is difficult to argue that an O- and F-contaminated flux-welded core shroud will not crack when a cold-worked surface layer is absent. Usually, the depth of intergranular cracking in a shroud weld far exceeds the thickness of the cold-worked layer, e.g., 15-30 mm[1] vs. 0.5-1.5 mm (Fig. 13). Although a cold-worked layer may accelerate crack nucleation and is known to exacerbate fluoride-assisted stress corrosion cracking,[7] it is difficult to explain the propagation of an intergranular crack in nonsensitized solution-annealed material that is free of martensite or ferrite film on the grain boundaries on the basis of a cold-worked layer alone.

Conclusions

1. Because of compelling economic advantages, large core internal components such as BWR core shrouds are welded in air by a shielded-metal or submerged-arc procedure in which welding flux compounds that contain CaF_2 are used to produce a plasma shield (weld fume) over the molten metal. Because of exposure to air and the weld fume, the heat-affected zones of the welds are significantly contaminated by O, F, and Ca, whereas contamination in a tungsten-inert-gas weld is negligible.

2. Impurity contamination and grain-boundary microstructure of a field-cracked Type 304L stainless steel BWR core shroud weld and of mockup shielded-metal-arc welds of Types 304L and Type 304 stainless steel were similar. As expected, grain boundaries of the heat-affected zones of the L-grade stainless steel core shroud weld were free of carbide, and neither martensite film nor grain-boundary Cr depletion was observed. Therefore, it is difficult to explain Type 304L stainless steel core shroud cracking on the basis of either classical intergranular stress corrosion cracking (driven by thermal sensitization) or irradiation-assisted stress corrosion cracking (driven by irradiation-induced Cr depletion).

3. Evidence shows that O concentration on grain boundaries of the heat-affected zone of a core shroud weld is higher than it is in grain matrices. As a result, more oxide particles precipitate on or near grain boundaries than in grain matrices.

4. Significant F contamination occurs in core shroud welds in association with O contamination, and F content in the heat-affected zone of a core shroud weld appears to be higher in the O-rich region beneath the weld scale and oxides. This explains well why weld scale and surface oxide layer strongly exacerbate the susceptibility of flux welds such as shielded-metal- or submerged-arc welds to fluorine-assisted intergranular stress corrosion cracking.

5. Fine Ca-oxyfluoride precipitates are formed near the fusion line in the heat-affected zone of a core shroud weld. The precipitation of Ca-oxyfluorides is promoted by the grinding procedure used to remove the surface weld scale and weld cusps between each welding pass. The precipitates are readily dissolved in the water, thereby releasing F ions into the water.

6. The failure of Type 304L SS core shroud welds can be explained by a model that is based on oxyfluorine-assisted stress corrosion cracking, in which a synergism among O, Cr, and F plays a primary role. Cracking mechanisms of Types 304 and 304L SS core shroud welds are essentially the same. According to the model, susceptibility to intergranular stress corrosion cracking in a core shroud weld is influenced strongly by the ratio of the concentration of Cr ions to the concentration of F ions in crack tip water. When the ratio, strongly influenced by O and F distributions in the heat-affected zone, is lower on grain boundaries than in grain matrices, the material is susceptible to intergranular stress corrosion cracking. The two essential and necessary conditions for the process to occur are material contamination by F and higher concentration of O on grain boundaries. The model predicts that cracking in a flux-welded core shroud weld could occur even in the absence of a cold-worked surface layer, although absence of a cold-worked layer would delay the onset of cracking.

Acknowledgments

The authors thank M. B. McNeil, T. F. Kassner, and W. J. Shack for helpful discussions, and L. J. Nowicki and W. F. Toter for contributions to the experimental efforts. This work was supported by the U.S. Nuclear Regulatory Commission, Office of Nuclear Regulatory Research.

References

1. R. M. Horn, G. M. Gordon, F. P. Ford, and R. L. Cowan, Nucl. Eng. Design 174 (1997) 313.
2. H. M. Chung, J. H. Park, W. E. Ruther, J. E. Sanecki, R. V. Strain, and N. J. Zaluzec, in Proc. 8th Intl. Symp. on Environmental Degradation of Materials in Nuclear Power Systems - Water Reactors, S. M. Bruemmer, ed., American Nuclear Society, La Grange Park, IL, 1997, p. 846-856.
3. J. M. Cookson, G. S. Was, and P. L. Andresen, in Proc. 7th Intl. Symp. Environmental Degradation of Materials in Nuclear Power Systems - Water Reactors, NACE International, Houston, 1995, p. 1109.
4. H. M. Chung, W. E. Ruther, J. E. Sanecki, A. G. Hins, N. J. Zaluzec, and T. F. Kassner, J. Nucl. Mater. 239 (1996) 61.
5. H. M. Chung, J. E. Sanecki, and F. A. Garner, in Effects of Radiation on Materials: 18th International Symposium, ASTM STP 1325, R. K. Nanstad et al., eds., American Society for Testing and Materials, Philadelphia, 1999, p. 647.
6. K. Shimizu, K. Kobayashi, G. E. Thompson, P. Skeldon, and G. C. Wood, J. Electrochem. Soc. 144 (1997) 418.
7. C. T. Ward, D. L. Mathis, and R. W. Staehle, Corrosion, 25 (1969) 394.
8. W. E. Berry, E. L. White, and W. K. Boyd, Corrosion 29 (1973) 451.
9. G. J. Theus and J. R. Gels, in Corrosion Problems in Energy Conversion and Generation, C. S. Tedmon, Jr., ed., The Electrochemical Society, Princeton, NJ, 1974, p. 384.

10. P. E. C. Bryant and P. R. Habicht, "Fluorine–Induced Intergranular Corrosion of Sensitized Austenitic and Austenoferritic Stainless Steels," Combustion Engineering Internal Report TIS–5065; also in Proc. IAEA Workshop on Stress Corrosion Cracking, March 29-31, 1976, Vienna, Austria.

11. M. Takemoto, T. Shonohara, M. Shirai, and T. Shinogaya, Mater. Perform. 24 (1985) 26.

12. F. Zucchi, G. Trabanelli, and G. Demertzis, Corrosion Sci. 28 (1988) 69.

13. C. K. Lee and H. C. Shih, Corrosion 52 (1996) 690.

14. N. C. Huang and Z. Nagy, J. Electrochem. Soc. 134 (1987) 2215.